

Chiral symmetry restoration effects onto the meson spectrum from a Dyson-Schwinger/Bethe-Salpeter approach

Reinhard Alkofer ^{1,*} Christian S. Fischer ^{2,3,†} and Fabian Zierler ^{4,5,6,‡}

¹*Institute of Physics, University of Graz, NAWI Graz, Universitätsplatz 5, 8010 Graz, Austria*

²*Institut für Theoretische Physik, Justus-Liebig-Universität Gießen, Heinrich-Buff-Ring 16, 35392 Gießen, Germany*

³*Helmholtz Forschungsakademie Hessen für FAIR (HFHF), GSI Helmholtzzentrum für Schwerionenforschung, Campus Gießen, Heinrich-Buff-Ring 16, 35392 Gießen, Germany*

⁴*Technical University of Munich, TUM School of Natural Sciences, Physics Department, James-Frank-Str. 1, 85748 Garching, Germany*

⁵*Centre for Quantum Fields and Gravity, Faculty of Science and Engineering, Swansea University, Singleton Park, SA2 8PP, Swansea, United Kingdom*

⁶*Department of Physics, Faculty of Science and Engineering, Swansea University, Singleton Park, SA2 8PP Swansea, Wales, United Kingdom*

Light meson spectra are studied in a Dyson-Schwinger/Bethe-Salpeter approach to QCD. By varying the interaction strength of three sets of models for the quark-antiquark interaction, the transition from the chiral symmetric to the chirally broken regime in the vacuum is studied. The simplest type of these models leads to degenerate meson spectra for a large domain of the strength parameter. The more sophisticated and thus more realistic models show significantly smaller parameter domains for which degenerate meson spectra are obtained. The underlying mechanism for obtaining and then lifting degeneracies is traced back to the location of the quark propagators' poles, in particular, whether they are beyond or within the domain of integration in the Bethe-Salpeter equation. In view of this mechanism the potential relation of the obtained degeneracies to the dynamical emergence of symmetries is discussed, adding thereby another point of view on the conjectured chiral spin symmetry of QCD in the temperature domain right above the crossover.

I. INTRODUCTION

Degeneracies of states are typically related to symmetries. Hereby the corresponding multiplets are used together with the quantum numbers of the states to infer the underlying symmetry transformations. A recent example is given by the observation of meson degeneracies in QCD lattice calculations at temperatures just above the crossover temperature T_χ [1] and their interpretation in terms of the so-called chiral spin symmetry, see [2, 3] and references therein.

This emergent symmetry raises immediately questions about its nature, first of all, because it goes beyond the symmetry of the free Dirac Lagrangian. A possible interpretation might be linked to the fact that the chiral spin symmetry is a symmetry of the purely chromoelectric part of QCD, for respective details see, e.g., [3], where it is also suggested that in a temperature range from T_χ to $\sim 3T_\chi$ strongly-interacting matter forms a fluid of hadrons with still quite strong interactions in between them.

Although the current knowledge indicates that chiral spin symmetry smoothly disappears above $\sim 3T_\chi$ it is noteworthy in this context that quite recently there has been found some evidence that QCD undergoes two crossovers, resp., phase transitions [4] with the second transi-

tion being related to the percolation properties of center vortices and thus to confinement. Hereby the higher transition temperature at $\sim 2T_\chi$ is not so far from the estimate for the temperature at which chiral spin symmetry ceases to be realized. In a very recently suggested related scenario [5] arguments for an intermediate phase of strongly-interacting matter in between the hadronic and the high-temperature phases have been provided. In this phase the thermal degrees of freedom of quarks behave as deconfined whereas the gluons are still confined within glueballs.

Furthermore, based on spatial and temporal lattice correlators as well as theoretical constraints like microcausality, the KMS condition, etc., the persistence of resonance-like structures in the pseudo-scalar channel also above T_χ has been demonstrated [6]. Hereby the authors of this study state explicitly that this is consistent with predictions based on an emergent chiral spin symmetry.

Given this situation a deeper insight into the nature of this emergent chiral spin symmetry is certainly desirable.

The starting point of our investigation is hereby the observation of degeneracies of meson spectra, or more precisely, how can degeneracies be obtained when taking the nature of mesons as quark-antiquark bound states into account. Are there degenerate spectra of mesons for certain types of quark-antiquark interactions? How do degeneracies depend on the interaction strength? Which quantum numbers are involved? The latter question is particularly interesting. Traditionally, the focus has been on chiral partners such as π , σ and ρ , a_1 . The degeneracy

* reinhard.alkofer@uni-graz.at

† christian.fischer@theo.physik.uni-giessen.de

‡ fabian.zierler@tum.de

of the latter has been flagged as an important signal for chiral symmetry restoration which can be extracted from the dilepton spectrum of a heavy-ion collision[7]. Chiral spin symmetry, however, involves a much larger set of degeneracies [3].

To contribute to the answers to these questions we will employ a Dyson-Schwinger/Bethe-Salpeter (DS/BS) approach and investigate the resulting meson bound states based on different interaction models. For simplicity, we restrict ourselves to the vacuum for the moment and defer a study at finite temperature to later work. The role of the symmetry restoring parameter is then shifted from temperature to corresponding model parameters for the interaction strength. While this setup is certainly not elaborate enough to allow for definite conclusions on the potential high temperature phase discussed in [3], it is interesting in itself and allows for the identification of potential underlying dynamical mechanisms beyond simple symmetry considerations. Quite surprisingly a full pattern of extended and partial degeneracies can be found. Even more astonishingly, these patterns start (or better end) at parameter values for which the quark propagators' poles enter the integration domain for the integrals appearing in the BS equation

This paper is organized as follows: In the next section we present three interaction models to be used first in the DS equation for the quark propagator. In Sect. III we briefly review the BS equation for pseudo-scalar, vector, scalar and axial-vector mesons including the implementation of the three model interactions. In Sect. IV we present numerical results, first, for the behavior of the quark propagators' low-lying poles, and second, for the resulting spectra of mesons. We will identify the occurrence and the lifting of degeneracies as a function of the used parameter sets and relate them to the locations of the quark propagators' poles. In the concluding section we will discuss the mechanism uncovered by our investigation as well its implication for the emergent chiral spin symmetry. In the appendix we provide several additional plots for the location of the quark propagator's poles.

II. DYSON-SCHWINGER EQUATION AND MODELS

We work in Euclidean spacetime. In this case bound states occur at $-M^2 = P^2 < 0$ and the BS equations used to calculate meson masses probe the quark propagator in a parabolic region of the complex plane, see e.g. [8] for an overview. The quark DS equation reads:

$$S^{-1}(p) = S_0^{-1}(p) + Z_{1F} C_F g^2 \int_q D^{\mu\nu}(k) \gamma^\mu S(q) \Gamma^\nu(q, p). \quad (1)$$

Here $S(p)$ denotes the quark propagator for quark momentum p , $\Gamma_\nu^\alpha(q, p)$ the quark gluon vertex for momenta q and p and $D_{\mu\nu}(k = p - q)$ the gluon propagator. The

notation \int_q is a short form of $\int d^4q/(2\pi)^4$. $S_0(p)$ is the bare quark propagator, Z_{1F} the multiplicative renormalization constant of the bare quark-gluon vertex, and C_F the Casimir of the fundamental representation taking the value 4/3 for SU(3).

The quark propagator's Dirac tensor structure can be decomposed into two terms, and thus the quark propagator as well as its inverse are described by two scalar dressing functions:

$$S^{-1}(p) = +i\gamma_\mu p^\mu A(p^2) + \mathbb{1}B(p^2), \quad (2)$$

$$S(p) = -i\gamma_\mu p^\mu \sigma_A(p^2) + \mathbb{1}\sigma_B(p^2). \quad (3)$$

The dressing functions of the inverse quark propagator are related to those of the quark propagator by

$$\sigma_A(p^2) = \frac{A(p^2)}{p^2 A^2(p^2) + B^2(p^2)} \equiv A(p^2)\sigma(p^2), \quad (4)$$

$$\sigma_B(p^2) = \frac{B(p^2)}{p^2 A^2(p^2) + B^2(p^2)} \equiv B(p^2)\sigma(p^2). \quad (5)$$

The quark mass function is then given by

$$M(p^2) = B(p^2)/A(p^2) = \sigma_B(p^2)/\sigma_A(p^2). \quad (6)$$

In the following we briefly describe the three interaction models studied in this work. Our choice is guided by considerations of simplicity and feasibility. However, all three model types have already been tested extensively in their capability to describe the QCD phase diagram and found to be qualitatively useful, see [9] for a review. Model III can even be seen as a (slightly simplified) vacuum version of semi-quantitative successful truncations that are employed to predict the location of the critical endpoint of QCD [10]. Thus while our study cannot anticipate more involved investigations using the most advanced truncation schemes at finite temperature and chemical potential available today [11–13] it serves as a starting point with the potential to add qualitative insights to the discussion on chiral spin symmetry.

A. Model I

The first and simplest model of interest is the interaction proposed in Ref. [14]. It is Gaussian-like suppressed in the ultraviolet momentum regime, but provides sufficient strength at small momenta to trigger dynamical chiral symmetry breaking:

$$Z_{1F} g^2 D^{\mu\nu}(k) \Gamma^\nu(q, p) \rightarrow Z_2^2 \mathcal{G}(k^2) D_{free}^{\mu\nu}(k) \gamma^\nu, \quad (7)$$

$$\mathcal{G}(k^2) = 4\pi^2 \frac{D_I}{\omega_I^6} k^4 e^{-\frac{k^2}{\omega_I^2}}. \quad (8)$$

Here, Z_2 is the renormalization constant of the quark propagator and $D_{free}^{\mu\nu}(k) = \left(\delta_{\mu\nu} - \frac{k_\mu k_\nu}{k^2}\right) \frac{1}{k^2}$. The parameter D_I has mass dimension two and ω_I has mass

D_I	1	0.926	0.854	0.818	0.749	0.682	0.617	0.555	0.494	0.436	0.380	0.327	0.302	0.277	0.253	0.230
ω_I	0.500	0.494	0.487	0.484	0.477	0.469	0.461	0.453	0.445	0.435	0.426	0.415	0.410	0.404	0.398	0.391
D_I/ω_I^2	4	3.8	3.6	3.5	3.3	3.1	2.9	2.7	2.5	2.3	2.1	1.9	1.8	1.7	1.6	1.5

TABLE I. Parameters used in model I. The units are GeV^2 for D_I and GeV for ω_I .

dimension one. \mathcal{G} stands for a dimensionless effective running coupling. Both parameters are associated with chiral symmetry breaking: D_I/ω_I^6 is a measure for the interaction strength, while ω_I is associated with a scale. In our study below we decrease both parameters simultaneously while keeping the ratio $D_I/\omega_I^6 = 64 \text{ GeV}^{-4}$ constant, see table I. The initial values $D_I = 1 \text{ GeV}^2$ and $\omega_I = 0.5 \text{ GeV}$ are taken from Ref. [14] and correspond to their $D = 16 \text{ GeV}^{-2}$ and $\omega = 0.5 \text{ GeV}$ at the physical point of the model.

In Sec. IV we present results for the quark propagators' poles in the chiral limit and for a small current quark mass $m[\mu = 19 \text{ GeV}] = 0.005 \text{ GeV}$ in a momentum subtraction scheme. All meson masses are calculated with the non-vanishing current quark mass.

For this interaction the quark propagator DSEs can be solved in the entire complex plane at high precision. We follow the approach of Ref. [15] and use pole-counting integrals to identify the pole locations in the complex plane. We remark that our results agree well with the ones reported in [15, 16] for this interaction.

B. Model II

A phenomenologically successful effective interaction for the light pseudo-scalar and vector mesons that also captures the correct ultraviolet behaviour of an effective running coupling is given by [17]:

$$\mathcal{G}(k^2) = \mathcal{G}_{\text{IR}}(k^2) + \mathcal{G}_{\text{UV}}(k^2), \quad (9)$$

$$\mathcal{G}_{\text{IR}}(k^2) = 4\pi^2 \frac{D_{II}}{\omega_{II}^6} k^4 e^{-\frac{k^2}{\omega_{II}^2}}, \quad (10)$$

$$\mathcal{G}_{\text{UV}}(k^2) = \frac{4\pi^2 \gamma_m \left(1 - \exp\left[-\frac{k^2}{4m_t}\right]\right)}{\frac{1}{2}k^2 \ln\left[\tau + \left(1 + \frac{k^2}{\Lambda_{QCD}^2}\right)^2\right]}. \quad (11)$$

The infrared term is identical to Eq. (7), while the ultraviolet term ensures the correct perturbative running of the solutions for the quark propagator. Hereby, γ_m is the anomalous dimension of the quark mass. For the choice of the technical parameters m_t , τ and Λ_{QCD} , see [17]. While the UV-part of this interaction is important for systematic reasons, it is known to change the resulting spectrum only slightly as compared to Model I. We therefore in addition employ a different strategy for variation of parameters: here we keep the interaction scale $\omega_{II} = 0.4 \text{ GeV}$ constant, and decrease the interaction strength starting from $D_{II} = 0.93 \text{ GeV}^2$, which is the physical point of

the model taken from [17], down to $D_{II} = 0.03 \text{ mGeV}^2$. All calculations have been performed with a current mass $m[\mu = 19 \text{ GeV}] = 3.7 \text{ MeV}$.

For both model I and model II the quark dressing function need only to be solved iteratively for positive real momenta squared $p^2 \geq 0$. Once they are accurately known there, the values of the dressing functions can be determined for complex values of p^2 without further need for iterative methods by simply calculating the right-hand-side of the respective integral equation. Note, however, that this is accidental. As has been noted already in [18], this procedure suffers from integrating over cuts produced in the angular integral of the quark self-energy. It so happens that these cuts are so small for the Model I and Model II that the corresponding errors are negligible. This is generically not the case and also does not work for Model III.

C. Model III

Our third model goes beyond truncations with models for the effective running coupling restricted to the quark sector of QCD. Instead, we solve the coupled set of DS equations for the quark, gluon and ghost propagator following the truncation of Ref. [19]. In general, the ghost and gluon propagators are represented by

$$D_{\mu\nu}(k) = \left(\delta_{\mu\nu} - \frac{k_\mu k_\nu}{k^2}\right) \frac{Z(k^2)}{k^2}, \quad (12)$$

$$D_G(k) = -G(k^2)/k^2, \quad (13)$$

where $Z(k^2)$ and $G(k^2)$ are the dressing functions of the gluon and ghost, respectively. We again use a rainbow-ladder type approximation for the full quark-gluon-vertex, but explicitly take into account a structure of the dressing function that is imposed by the corresponding Slavnov-Taylor identity (see [19, 20] for details):

$$\Gamma^{\nu,a}(q,p) = \frac{igZ_2}{Z_{1F}} T^a \gamma_\nu G^2(k^2) A(k^2), \quad (14)$$

where $k = p - q$ is the gluon momentum. In the notation of Eq.(7) this results in an effective running coupling

$$\mathcal{G}(k^2) = \frac{1}{Z_2} g^2 G^2(k^2) Z(k^2) A(k^2) \quad (15)$$

which is invariant under changes of renormalization similar to models I and II.

In order to again explore the model at different interaction-strengths, we multiply the coupling by a scale

dependent strength-parameter $h(k^2, D_{III})$, that preserves the UV physics while providing damping in the IR:

$$g^2 \rightarrow g^2 h(k^2, D_{III}), \quad D_{III} \in [0, 1],$$

$$h(k^2, D_{III}) = \arctan\left(\frac{k^2}{10}\right) \frac{2}{\pi} (1 - D_{III}) + D_{III}. \quad (16)$$

For our results in section IV we vary D_{III} between $D_{III} = 1$ and $D_{III} = 0.1$. For model III all calculations have been performed with a current quark mass $m[\mu = 31 \text{ GeV}] = 1.9 \text{ MeV}$.

In this approach every Yang-Mills dressing function remains purely real. In order to solve the quark DS equation we pursue the same approach as in Ref. [19]: First solve all propagator DS equations self-consistently on the real semi-positive half-axis, i.e., for $p^2 \in \mathbb{R}$, $p^2 \geq 0$. This procedure also fixes all renormalization constants. Then, we solve the momentum shifted equation, i.e., we substitute $q \rightarrow p - q$. The Yang-Mills propagators then only depend on the real new loop momentum q , ($G(q^2)$, $Z(q^2)$), whereas the internal quark propagator carries the momentum difference $k = p - q$. The resulting equation can then be solved on a momentum grid with parabola shape in the complex momentum plane.

III. MESON BOUND STATES AND BETHE-SALPETER EQUATIONS

As already stated above for all three models we use a rainbow-ladder type truncation of the quark propagator DS and meson BS equations. In this section we briefly review some aspects of the BS equation for mesons which are of particular relevance for the study presented here, for more details about the BS equation and its use in hadron physics we refer, e.g., to the review [8].

The Bethe-Salpeter equation for quark-antiquark states can be written as

$$[\Gamma^{(\mu)}(p, P)]_{tu} = \int_q K_{tu,rs}(q, p, P) [S(q_+) \Gamma^{(\mu)}(q, P) S(q_-)]_{sr}, \quad (17)$$

with generic indices for color, flavor and Dirac structures of the interaction kernel $K(q, p, P)$. The BS-amplitude $\Gamma^{(\mu)}(p, P)$ depends on the total momentum P of the meson and the relative momentum p of the quark-antiquark pair. The BS equation can be solved numerically as eigenvalue equation of the form $\lambda(P^2) \Gamma = (K S_+ S_-) \cdot \Gamma$ with $S_{\pm} = S(q_{\pm})$. Note that the momenta $q_{\pm} = q \pm P/2$ appearing as arguments of the quark propagators are complex, since in the rest frame of the meson we have $P = (0, 0, 0, iM)$ with meson mass $-P^2 = M^2$. Evaluating q_{\pm}^2 one finds that the region of complex momenta needed to solve the BS-equation is bounded by a parabola with the real line as symmetry axis and with the apex at $-M^2/4$, M denoting the respective meson's bound state mass. In practice, one solves the DS-equation in the complex momentum plane once on a parabola with maximal

possible \mathcal{M} such that poles in the quark propagator are not encountered inside the parabola. In turn this means that using this quark propagator, the BS-equation can be explored for all mesons with masses $M \leq \mathcal{M}$ without additional extrapolations in the eigenvalue. This is indeed all we need for this work.

Depending on the quantum numbers of the meson in question, the amplitude $\Gamma^{(\mu)}$ carries different Dirac structures. For pseudoscalar (P) and scalar (S) mesons with quantum numbers $J^{PC} = 0^{-+}$ and $J^{PC} = 0^{++}$ in vacuum the Dirac tensor decomposition of the BS-amplitudes is given by

$$\Gamma_P(p, P) = \gamma_5 \left\{ E_P(p, P) - i \not{P} F_P(p, P) - i \not{p} P \cdot p G_P(p, P) + [\not{P}, \not{p}] H_P(p, P) \right\}, \quad (18)$$

$$\Gamma_S(p, P) = \mathbb{1} \left\{ E_S(p, P) - i \not{P} P \cdot p F_S(p, P) - i \not{p} G_S(p, P) + [\not{P}, \not{p}] H_S(p, P) \right\}. \quad (19)$$

The corresponding flavor and color parts of the amplitudes can be found in Ref. [8] together with details on the underlying construction principles as well as explicit expressions for parity and charge conjugation operations. In general, the γ_5 -factor of the pseudoscalar mesons accounts for parity, whereas extra factors $P \cdot p$ at some places ensure that all BSA components E_X , F_X , G_X , and H_X with $X \in \{P, S\}$ transform similarly under charge conjugation. Furthermore, the signs are chosen such that all BSA components are positive.

For the vector (V) and axial-vector (A) meson with quantum numbers $J^{PC} = 1^{--}$ and $J^{PC} = 1^{+-}$ as well as $J^{PC} = 1^{++}$ in vacuum we work with the tensor decomposition

$$\Gamma_V^\mu(p, P) = i\gamma_\tau^\mu F_{1V}(p, P) + \gamma_\tau^\mu \not{P} F_{2V}(p, P) + (p_\tau^\mu \mathbb{1}_D - \gamma_\tau^\mu \not{p}) P \cdot p F_{3V}(p, P) + (i\gamma_\tau^\mu [\not{P}, \not{p}] + 2ip_\tau^\mu \not{P}) F_{4V}(p, P) + p_\tau^\mu \mathbb{1}_D F_{5V}(p, P) + ip_\tau^\mu \not{P} P \cdot p F_{6V}(p, P) - ip_\tau^\mu \not{p} F_{7V}(p, P) + p_\tau^\mu [\not{P}, \not{p}] F_{8V}(p, P),$$

$$\Gamma_A^\mu(p, P) = \gamma_5 \left\{ i\gamma_\tau^\mu F_{1A}(p, P) + \gamma_\tau^\mu \not{P} P \cdot p F_{2A}(p, P) + (p_\tau^\mu \mathbb{1}_D - \gamma_\tau^\mu \not{p}) F_{3A}(p, P) + (i\gamma_\tau^\mu [\not{P}, \not{p}] + 2ip_\tau^\mu \not{P}) F_{4A}(p, P) + p_\tau^\mu \mathbb{1}_D P \cdot p F_{5A}(p, P) + ip_\tau^\mu \not{P} P \cdot p F_{6A}(p, P) - ip_\tau^\mu \not{p} F_{7A}(p, P) + p_\tau^\mu [\not{P}, \not{p}] P \cdot p F_{8A}(p, P) \right\}, \quad (20)$$

which is constructed such that the on-shell (axial-)vector meson is transverse to its total momentum P . The subscript τ indicates transversality of $w \in \{\gamma, p\}$ w.r.t. the total momentum, i.e., $w_\tau^\mu = T_{\mu\nu}(P) w^\nu$. The two different charge conjugation eigenstates of the axialvector mesons corresponding to the $a1$ and $b1$ states in nature show up with masses close to each other in the numerical solutions of the corresponding BS-equation. They are conveniently

distinguished using a Chebychev expansion of the $p \cdot P$ -dependence of the dressing functions F_{iA} and taking into account only contributions even or odd in powers of $p \cdot P$.

Finally, we have to specify the scattering kernel K in the Bethe-Salpeter equation. It cannot be chosen arbitrarily, but it has to match the truncation scheme used in the DSE such that the axialvector Ward-Takahashi identity is satisfied and the (pseudo-)Goldstone nature of the pion preserved. Corresponding details and an explicit derivation of this property can be found, e.g., in Ref. [8]. For the rainbow-ladder truncation, this is achieved by using a single effective gluon exchange between two bare vertices

$$K_{tu,rs}(p, q, P) = -C_f Z_2^2 [\gamma^\mu]_{tu} [\gamma^\nu]_{rs} \mathcal{G}(k^2) D_{free}^{\mu\nu}(k), \quad (21)$$

with the same effective running coupling \mathcal{G} as the one in the quark self-energy detailed above for our models I-III.

IV. NUMERICAL RESULTS

In the following we will detail our results for the analytic structure of the quark propagator and the masses of (pseudo-)scalar and (axial-)vector mesons as a function of the interaction strength in all three models I-III. We first discuss the pole structure of the quark propagator, but ask the reader to keep in mind that we will subsequently establish a direct connection to the emerging meson masses and mass degeneracies.

A. Pole structure of the quark propagator

When solving the respective DS equations we note that in all three models we find a qualitatively similar analytic structure of the quark propagator as a function of interaction strengths. The quark DS equation for models I and II can be solved in the entire complex plane. For model I, we can even closely track the poles by computing the associated pole-counting integrals, and determine the multiplicity of poles. In model III, we find that we can solve the DSEs self-consistently beyond the occurrence of the first pole, as long as the first pole is real. However, our system of DSEs fails to converge if the set of external momenta contains a complex pole.

For very small strength parameters $D_{I,II,III}$ we always find a real-valued pole of the quark propagator at or close to the origin. The typical momentum scale of the pole is of the order of the current quark mass, $p^2 \sim -m^2$ with $m \rightarrow 0$ in the chiral limit. This is, of course, what is expected when the interaction strength is not large enough to trigger dynamical chiral symmetry breaking. In model I and II, we observe that the next closest pole is actually a degenerate pair of real-valued poles. We can only conjecture that this behavior persists for model III, but we do not have numerical evidence.

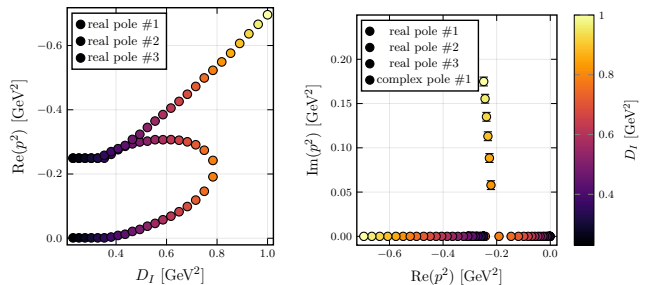


FIG. 1. (left) The location of the poles of the function $\sigma(p^2)$ (4) for model I in the complex p^2 -plane as a function of D_I , cf. table I. (right) Position of the poles of $\sigma(p^2)$ along the real axis as a function of D_I . When the two low-lying poles cross they generate a pair of complex conjugate poles, cf. the left panel. Note, that we also observe a crossing of two real valued poles that does not lead to the formation of a complex pole pair.

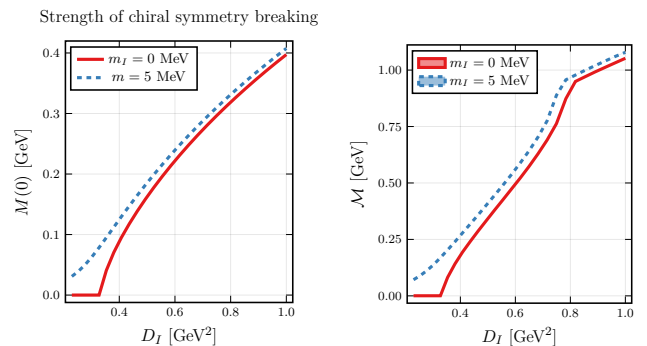


FIG. 2. (left) Displayed is the infrared value of the quark mass function $M(0)$, as a proxy for the strength of dynamical chiral symmetry breaking, for model I as function of D_I in the chiral limit and for a small quark current mass. (right) The parameter \mathcal{M} determined by the largest parabola with apex $-\mathcal{M}^2/4$ that is free of poles for the given coupling strength D_I . In the presence of non-vanishing current quark masses, the second-order transition, visible in both variables, is smoothened into a crossover behavior.

The first pole remains close to the origin until either $D_{I,II,III}$ is large enough to trigger dynamical chiral symmetry breaking. At this point the lowest-lying pole starts to move along the real axis deeper into the timelike momentum region. For model I and II, we observe that the degeneracy in the next real pole pair is lifted as chiral symmetry gets broken. Eventually, one of the poles moves towards the origin while the other one moves even deeper into the timelike region.

For all three models we observe that two lowest-lying real poles will eventually “collide” on the real axis, and form a complex conjugate pair of poles. In model I, we are able to see this effect repeated at a larger strength parameters. NB: A similar behavior of real poles colliding and forming pairs of complex conjugated poles has been observed when tuning the quark mass in Ref. [15].

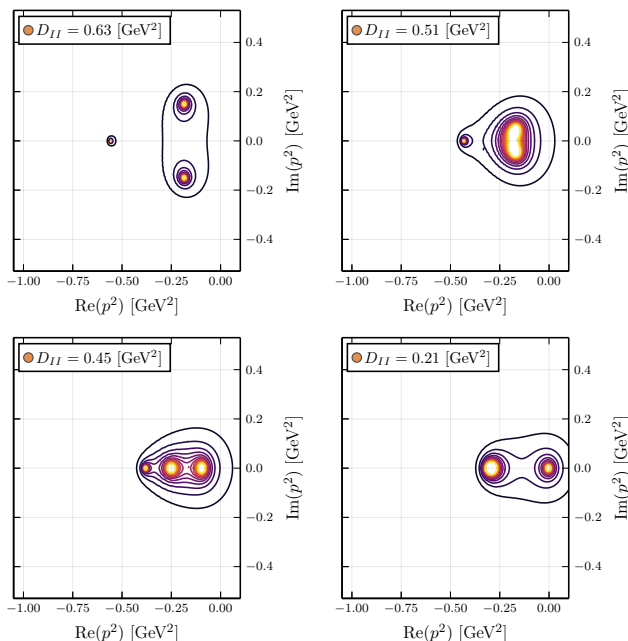


FIG. 3. Pole structure emerging from model II as a function of the strength parameter D_{II} for fixed $\omega_{II} = 0.4$ GeV. We observe a pattern similar to the one of model I.

For illustrating the above described pattern of dependencies of pole locations w.r.t. the interaction strength we focus first on the simplest interaction model, i.e., model I in the chiral limit. In Fig. 1 we show the positions of the three lowest-lying quark propagator's poles for complex values of p^2 (= closest to the origin) for massless quarks, color coded according to the corresponding value of the strength parameter D_I . The pole locations are determined by the zeros of the denominators of the function $\sigma_A(p^2)$ (4) or, equivalently, $\sigma_B(p^2)$ (5). Poles in the dressing functions $A(p^2)$ and/or $B(p^2)$ are irrelevant, since they appear much further out in the time-like momentum plane. At $D_I = 0.23$ GeV² we start with only two pole locations at $p^2 = 0$ and $p^2 = -0.249$ GeV², since the latter location accommodates the pair of degenerate poles already discussed above. For $D_I/\omega_I^2 \geq 1.92$ (corresponding roughly to $D_I \approx 0.332$ GeV²) dynamical chiral symmetry breaking occurs leading to the split-up of the degenerate poles as visible in the right diagram of Fig. 1. At this point the quark mass function $M(p^2) = B(p^2)/A(p^2)$ starts to be non-vanishing also in the chiral limit. In the left panel of Fig. 2 we display the corresponding value of $M(0)$ as function of the strength parameter D_I . In the chiral limit, the transition is a second order (quantum) phase transition, whereas at finite quark current quark masses it becomes a cross-over as also displayed in this figure.

As already discussed above, the poles begin to move with increasing interaction strength but stay real in the interval $0.332\text{GeV}^2 \leq D_I \leq 0.801\text{GeV}^2$. As can be seen from Fig. 1, two poles merge at the upper end of this in-

terval and they split up into a pair of complex-conjugated poles when further increasing the interaction strength. The appearance of complex-conjugated poles does not have any visible effect on the quark propagator dressing functions for Euclidean momenta. As can be seen in the left panel of Fig. 2 $M(0)$ is a smooth function of the interaction strength D_I in the respective region.

In the right panel of Fig. 2 we show the parameter \mathcal{M} defined via the largest parabola with the real axis as symmetry axis and an apex at $-\mathcal{M}^2/4$ that remains free of poles, cf. our discussion below Eq. (17). Of course, by construction \mathcal{M} shows a cusp when the complex-conjugated pole pair appears, since then the real part of the pole location hardly changes whereas mainly the imaginary part grows leading only to slight larger possible parabolas with growing interaction strength.

For further illustration we also show the pole positions in the complex momentum plane for four selected values of the interaction strength D_{II} of model II in Fig. 3. In the lower right panel, the interaction strength is subcritical, and therefore the quark propagator possesses a pole at the origin and a double pole at finite p^2 . Increasing the interaction strength one has, as in model I, first three real poles (lower left panel) and then one pair of complex-conjugated poles and a real pole (upper panels). The main difference is that also $\mathcal{G}_{UV}(k^2)$ (11) provides some interaction strength, and therefore dynamical chiral symmetry breaking and pole merging happen at respective smaller values of the IR interaction strength.

B. Meson mass degeneracies

When solving the meson BS equations for varying interaction strengths we noticed a very interesting general pattern, see Fig. 4. For small values of the interaction strength we observed degeneracies in the low-energy meson spectrum. Furthermore, these degeneracies appear to be linked to the position of the quark propagator's closest pole to the origin. The observed degeneracies are hereby qualitatively similar in all three models and differ only somewhat quantitatively.

For a detailed discussion let us start at the physical point, i.e., at maximal interaction strength. All three diagrams in Fig. 4 show the masses of mesons with quantum numbers $J^{PC} = 0^{-+}, 0^{++}, 1^{--}, 1^{++}, 1^{+-}$ in the respective models and with current quark masses adapted to reproduce the experimental value of the mass of the pion. As is typical for rainbow-ladder type approximations, the vector meson masses are not too far away from their experimental value (although there is no width), whereas the masses of the scalar meson and the axialvectors are far off. This is well-known and discussed in detail e.g. in Ref. [8]. Beyond rainbow-ladder truncations (partly) remedy this situation. However, these require orders of magnitude more numerical effort and are therefore currently not feasible for the purpose of this exploratory work. We believe these are also not necessary, since we

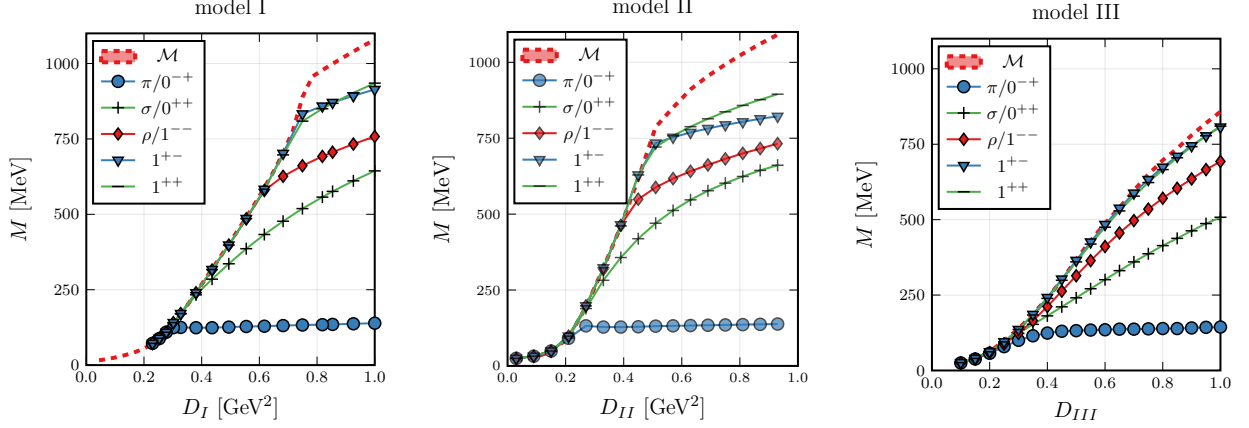


FIG. 4. Masses of mesons with quantum numbers $J^{PC} = 0^{-+}, 0^{++}, 1^{-}, 1^{++}, 1^{+-}$ as functions of the strength parameters $D_{I,II,III}$ of models I-III. In all cases we obtain the same pattern of degeneracy at small interaction strengths. Shown is furthermore the parameter \mathcal{M} characterizing the largest parabolic region symmetric to real p^2 with apex $-\mathcal{M}/4$.

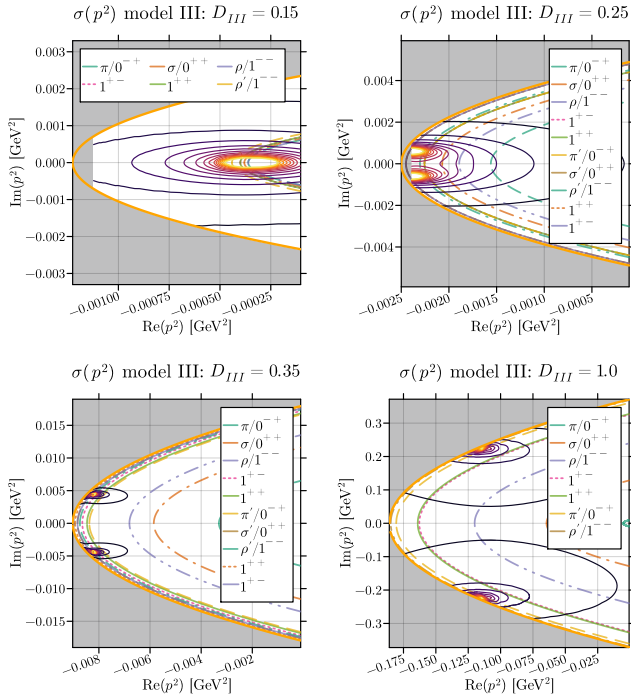


FIG. 5. Dressing function $\sigma(p)$ for model III based on the ghost and gluon propagators on the real axis for various strength parameters D_{III} . The plot shows the largest parabola for which we could solve the complex quark DSEs self-consistently, as well as the parabolas associated with the meson masses as determined through their respective BSEs.

are mainly interested in emerging general properties such as degeneracy patterns and their relations to analytical structure. This purpose is served, to our mind, by the available models.

Lowering the interaction strength we observe a similar pattern in all three models. First the two axialvector

states become degenerate (if not already from the start), then the vector mesons join, then the scalar meson for even lower interaction strength and finally also the pion becomes mass degenerate with the others once chiral symmetry is restored. While the latter phenomenon is naturally explained by chiral symmetry restoration, the approximate degeneracy of the other chiral partners, the vector meson (the ρ) and the 1^{+-} (the a_1), already happens at much larger values of the interaction strength. Furthermore, the extension of the symmetry to the scalar state and the other axialvector is not explained by the ‘conventional’ notion of chiral partners. Such extended degeneracy multiplets, however, have only been postulated in chiral spin symmetry scenarios [2, 3] in the context of finite temperature QCD.

It is also very interesting to compare this emerging pattern of degeneracies with the size of the parabola characterised by \mathcal{M} , also shown in the plots. Most directly for model I, but also visible for models II and III we observe that the degeneracy pattern seems to be driven by the (real) pole locations of the quark propagator. Once the interaction strength is small enough that the pair of complex conjugate poles hit the real axis (indicated by the kink in \mathcal{M} , cf. Fig. 2), the movement of the location of the pole towards the origin forces the mass curves to compress and become degenerate. A possible explanation for this behaviour is given in the summary. In any case, to our knowledge this link between analytic structure and mass degeneracies has not been observed before and constitutes a potential new aspect in the discussion of chiral spin symmetry scenarios [2, 3].

Finally, in model III we also studied the fate of radially excited states. In Figs. 5 we show both the pole structure and the parabolas corresponding to the meson masses as determined through the BSEs. The masses for the ground states are the same as displayed in Fig. 4, but we also show the corresponding parabolas for the first radial excitations. For small values of the strength parameter

D_{III} the respective first excited states are right above the ground states and (at least partly depending on the value of D_{III}) degenerate within numerical accuracy. The same presentation for more values of D_{III} are collected in appendix A.

V. CONCLUSION

Herein we studied the location of the low-lying quark propagator’s poles and the low-lying meson spectrum in three interaction models within the DS-BS approach. These three models are of different sophistication and formulated such that the interaction strength in the sub-GeV region can be controlled by a single parameter.

A solution of the DS and BS equations in rainbow-ladder truncation reveals several degeneracy patterns in the meson spectrum at small interaction strengths. For an interaction strength which is too small to trigger dynamical chiral symmetry breaking the observed degeneracies are no surprise but the expected ones. For interaction strengths right above the critical one, however, the observed degeneracies are not at all anticipated. We note that with increasing complexity of the model the parameter regions where these degeneracies are observed gets smaller, however, these degeneracies are observed for all three models. More importantly, the degenerated meson mass is closely related to the location of the lowest-lying pole of the quark propagator.

The latter observation can be traced back to the mathematical properties of the BS equation in ladder approximation. The respective BS kernel contains two quark propagators, and therefore if the integration region comes close to a pole of the quark propagator this close-by subregion provides a large if not the dominating contribution. (NB: This mechanism of dominating sub-regions close to poles is at work independently of whether the poles are located on the real axis or occur as pairs of complex-conjugated poles.) Therefore, independent of the quantum number of the mesons and thus the details of the BS kernel similarly large contributions will be picked up in the integrand.

Due to this, the degeneracies in the meson spectrum are caused by the analytic structure of the BS kernel irrespective of any symmetry considerations.

We want to note that “explanations” based on the analytic structure are quite common. E.g., the so-called Silver blaze property [21–24], which states that in quantum systems at non-vanishing density observables can only change with density if the chemical potential exceeds the mass of the lightest excitation, can be traced back to the fact that values of certain integrals only vary if the analytic properties of the integrands are modified, cf. Sect. 7 of [25].

For QCD at vanishing temperature and density the strength of the quark-gluon interaction, e.g., in the Lan-

dau gauge, is of a given certain momentum-dependence and strength. (NB: As the full quark-gluon vertex is highly non-trivial also other couplings than the vector one play an important role.) Increasing the temperature due to slightly above the chiral crossover temperature will come with a substantial weakening of the infrared strength of the interaction. And as a matter of fact one observes then in lattice calculations degeneracies between, e.g., the vector and axialvector correlators, see, e.g., [1].

In view of the results presented here a re-examination of these observed degeneracies with respect of their relation to the analytic properties of the quark propagator and bound state kernels at these temperatures seems worthwhile. Such an investigation may well add to a further understanding of the physics and symmetries of strongly interacting matter in the temperature regime around and slightly above the chiral crossover.

ACKNOWLEDGMENTS

We are grateful to Owe Philipsen and Lorenz von Smekal for fruitful discussions.

F.Z. is supported by the STFC Consolidated Grant No. ST/X000648/1 and acknowledges support from the Advanced ERC grant ERC-2023-ADG-Project EFT-XYZ.

CF acknowledges support by the Deutsche Forschungsgemeinschaft (DFG, German Research Foundation) through the Collaborative Research Center TransRegio CRC-TR 211 “Strong-interaction matter under extreme conditions”.

Open Access Statement—For the purpose of open access, the authors have applied a Creative Commons Attribution (CC BY) licence to any Author Accepted Manuscript version arising.

Research Data Access Statement—The code and data used to generate the plots and tables in this manuscript can be downloaded from Ref. [26].

Appendix A: More plots and tables of the pole structure

We show plots of the pole structure of all parameters investigated in this work. In Fig. 6 we show the plots of the pole structure for model II, and in Fig. 7 we show plots for model III. We further tabulate all data depicted in Fig. 4 in Tabs. II and III.

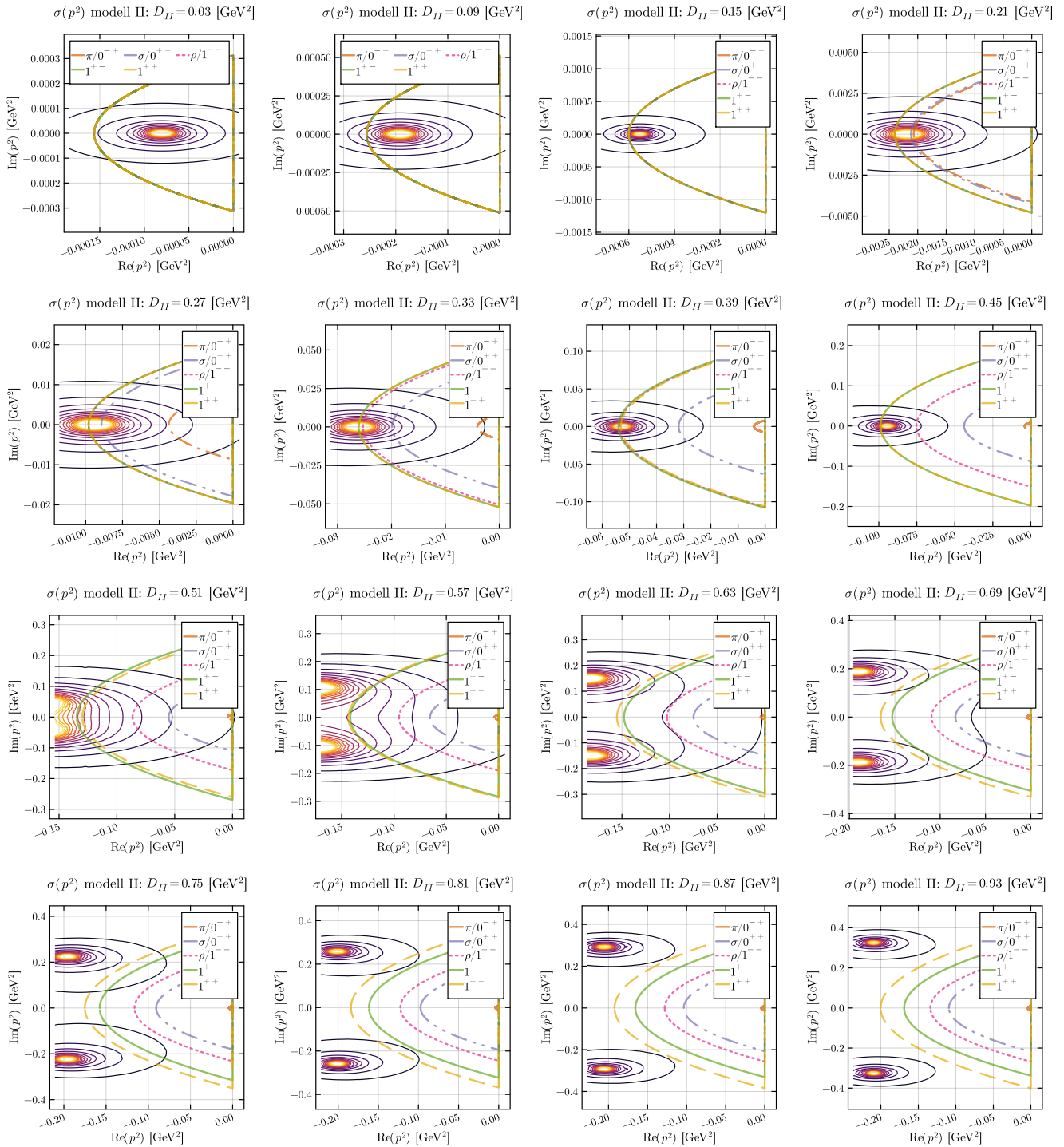


FIG. 6. Dressing function $\sigma(p)$ for model II based on the Maris-Tandy interaction for a fermion mass of 3.7 MeV. The model parameter $\omega_{II} = 0.4$ GeV is fixed while the parameter D_{II} is varied. We show the parabolas corresponding to the meson masses as determined through their respective BSEs.

[1] C. Rohrhofer, Y. Aoki, G. Cossu, H. Fukaya, C. Gatttringer, L.Y. Glozman et al., *Symmetries of*

spatial meson correlators in high temperature QCD, *Phys. Rev. D* **100** (2019) 014502 [1902.03191].

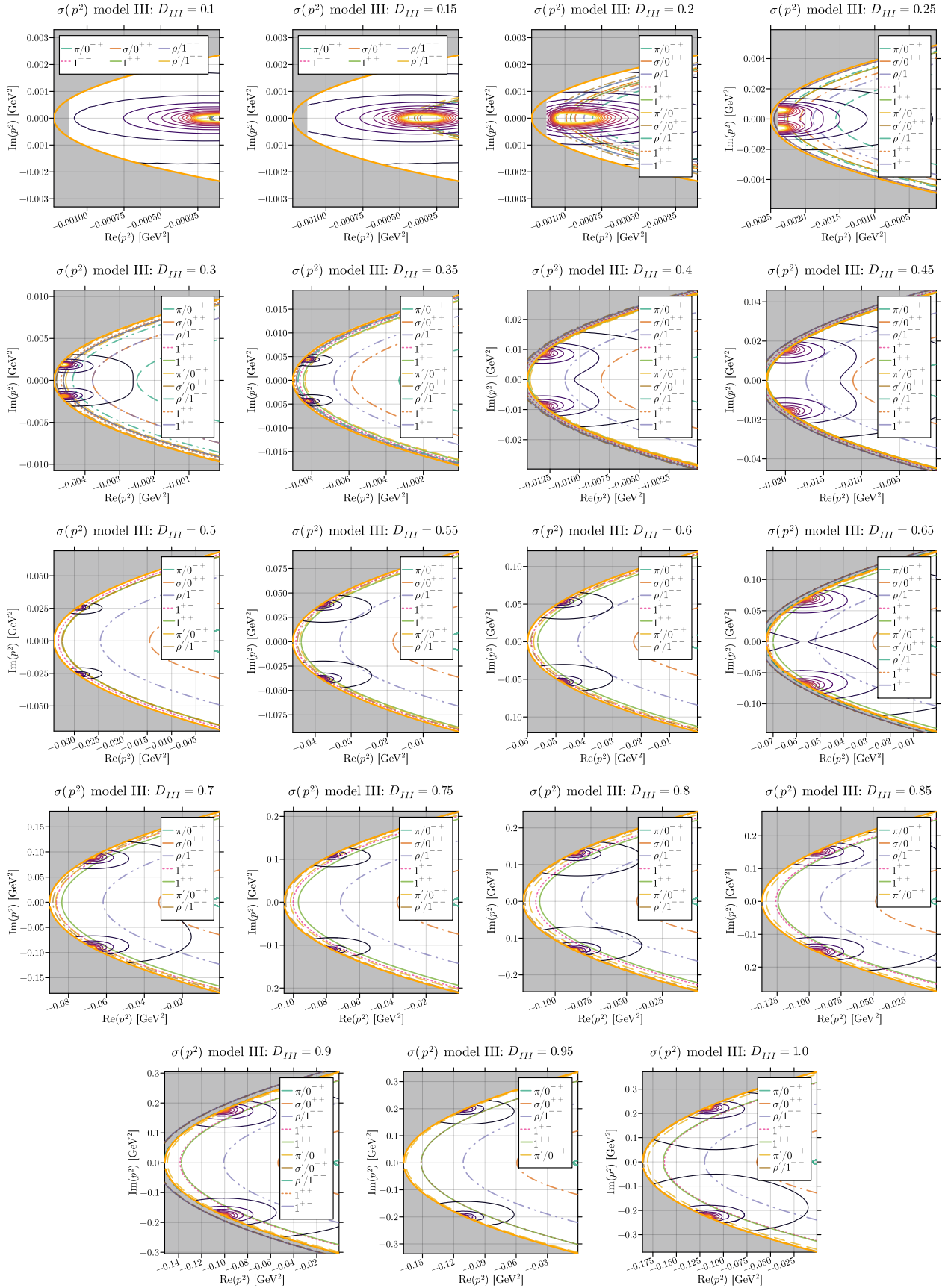


FIG. 7. Dressing function $\sigma(p)$ for model III based on the ghost and gluon propagators on the real axis for various strength parameters D_{III} . The plot shows the largest parabola for which we could solve the complex quark DSEs self-consistently, as well as the parabolas associated with the meson masses as determined through their respective BSEs. For $D_{III} < 0.2$ we can extend the parabolic region in the DSE iteration procedure and retain convergence.

TABLE II. (left) Tabulated values of the meson masses extracted from the BSEs for model I set to a physical scale (MeV) and the corresponding parameter \mathcal{M} . (right) Tabulated values of the meson masses extracted from the BSEs for model II set to a physical scale (MeV) and the corresponding parameter \mathcal{M} .

D_I	$m(0^{-+})$	$m(0^{++})$	$m(1^{--})$	$m(1^{+-})$	$m(1^{++})$	\mathcal{M}
0.230	72	72	73	72	72	72
0.253	88	88	89	89	89	89
0.277	109	110	109	109	109	111
0.302	124	140	141	141	141	137
0.327	125	170	171	171	171	169
0.380	124	233	240	240	240	240
0.436	124	285	315	317	317	318
0.494	126	336	398	398	398	402
0.555	128	386	485	486	486	490
0.617	129	433	579	583	583	588
0.682	131	477	626	702	697	703
0.749	133	519	661	833	809	889
0.818	134	557	692	859	850	978
0.854	135	576	706	871	868	999
0.926	137	611	733	893	903	1040
1.0	139	644	758	914	935	1080

D_{II}	$m(0^{-+})$	$m(0^{++})$	$m(1^{--})$	$m(1^{+-})$	$m(1^{++})$	\mathcal{M}
0.03	25	25	25	25	25	18
0.09	32	32	32	32	32	28
0.15	49	49	49	49	49	47
0.21	91	92	98	98	98	94
0.27	132	189	198	198	198	194
0.33	128	282	318	323	323	324
0.39	128	357	463	465	461	460
0.45	129	419	549	629	629	616
0.51	131	470	588	734	721	787
0.57	132	512	617	753	758	851
0.63	133	547	641	769	788	911
0.69	134	577	662	782	814	955
0.75	135	602	682	794	837	993
0.81	136	624	700	804	858	1028
0.87	137	644	716	814	877	1061
0.93	138	661	732	822	895	1091

TABLE III. Tabulated values of the meson masses extracted from the BSEs for model III set to a physical scale (MeV) and the corresponding parameter \mathcal{M} . In some cases, indicated by a $-$ sign, we have not been able to extract the on-shell masses of the first radial excitations within numerical accuracy. In principle those could be extracted using well-established extrapolation procedures in the eigenvalue curves. However, since these are not the main topic of this work and the general trend can already be seen from the available data, we did not invest the (considerable) CPU-time.

D_{III}	$m(0^{-+})$	$m(0^{++})$	$m(1^{--})$	$m(1^{+-})$	$m(1^{++})$	$m(0^{-+'})$	$m(0^{++'})$	$m(1^{--'})$	$m(1^{+-'})$	$m(1^{++'})$	\mathcal{M}
0.1	25	26	25	26	26	-	-	27	-	-	21
0.15	38	39	38	40	40	-	-	42	-	-	39
0.2	57	61	59	62	62	63	66	65	63	65	62
0.25	79	91	87	95	95	95	99	96	99	99	99
0.3	100	123	123	136	136	135	139	132	137	136	138
0.35	115	153	165	186	184	183	188	187	189	188	187
0.4	124	181	212	242	239	238	246	240	244	245	240
0.45	130	211	263	303	299	299	306	301	307	307	300
0.5	132	241	314	365	360	360	-	361	-	-	368
0.55	134	271	364	426	419	421	-	424	-	-	430
0.6	135	301	411	484	475	481	-	485	-	-	488
0.65	137	331	456	538	529	537	551	543	551	550	540
0.7	137	360	497	588	578	589	-	594	-	-	597
0.75	138	387	535	633	623	638	-	647	-	-	650
0.8	139	414	571	674	666	687	-	696	-	-	697
0.85	139	438	604	710	705	731	-	-	-	-	736
0.9	141	463	635	745	742	774	797	782	799	799	780
0.95	143	487	666	778	778	815	-	-	-	-	820
1	144	508	693	807	810	850	-	860	-	-	858

- [2] L.Y. Glozman, O. Philipsen and R.D. Pisarski, *Chiral spin symmetry and the QCD phase diagram*, *Eur. Phys. J. A* **58** (2022) 247 [2204.05083].
- [3] L.Y. Glozman, *Chiral spin symmetry and hot/dense QCD*, *Prog. Part. Nucl. Phys.* **131** (2023) 104049 [2209.10235].
- [4] J.A. Mickle, C. Allton, R. Bignell and D.B. Leinweber, *Center vortex evidence for a second finite-temperature QCD transition*, *Phys. Rev. D* **111** (2025) 034508 [2411.19446].
- [5] Y. Fujimoto, K. Fukushima, Y. Hidaka and L. McLerran, *A New State of Matter between the Hadronic Phase and the Quark-Gluon Plasma?*, 2506.00237.
- [6] P. Lowdon and O. Philipsen, *Spectral properties of pseudo-scalar mesons through the QCD chiral crossover*, *J. Subatomic Part. Cosmol.* **3** (2025) 100063 [2412.08371].
- [7] R. Rapp and J. Wambach, *Chiral symmetry restoration and dileptons in relativistic heavy ion collisions*, *Adv. Nucl. Phys.* **25** (2000) 1 [hep-ph/9909229].
- [8] G. Eichmann, H. Sanchis-Alepuz, R. Williams, R. Alkofer and C.S. Fischer, *Baryons as relativistic three-quark bound states*, *Prog. Part. Nucl. Phys.* **91** (2016) 1 [1606.09602].
- [9] C.S. Fischer, *QCD at finite temperature and chemical potential from Dyson-Schwinger equations*, *Prog. Part. Nucl. Phys.* **105** (2019) 1 [1810.12938].
- [10] C.S. Fischer, J. Luecker and C.A. Welzbacher, *Phase structure of three and four flavor QCD*, *Phys. Rev. D* **90** (2014) 034022 [1405.4762].
- [11] W.-j. Fu, J.M. Pawłowski and F. Rennecke, *QCD phase structure at finite temperature and density*, *Phys. Rev. D* **101** (2020) 054032 [1909.02991].
- [12] F. Gao and J.M. Pawłowski, *Chiral phase structure and critical end point in QCD*, *Phys. Lett. B* **820** (2021) 136584 [2010.13705].
- [13] P.J. Gunkel and C.S. Fischer, *Locating the critical endpoint of QCD: Mesonic backcoupling effects*, *Phys. Rev. D* **104** (2021) 054022 [2106.08356].
- [14] R. Alkofer, P. Watson and H. Weigel, *Mesons in a Poincare covariant Bethe-Salpeter approach*, *Phys. Rev. D* **65** (2002) 094026 [hep-ph/0202053].
- [15] A. Windisch, *Analytic properties of the quark propagator from an effective infrared interaction model*, *Phys. Rev. C* **95** (2017) 045204 [1612.06002].
- [16] S.M. Dorkin, L.P. Kaptari, T. Hilger and B. Kampfer, *Analytical properties of the quark propagator from a truncated Dyson-Schwinger equation in complex Euclidean space*, *Phys. Rev. C* **89** (2014) 034005 [1312.2721].
- [17] P. Maris and P.C. Tandy, *Bethe-Salpeter study of vector meson masses and decay constants*, *Phys. Rev. C* **60** (1999) 055214 [nucl-th/9905056].
- [18] P. Maris, *Confinement and complex singularities in QED in three-dimensions*, *Phys. Rev. D* **52** (1995) 6087 [hep-ph/9508323].
- [19] C.S. Fischer, P. Watson and W. Cassing, *Probing unquenching effects in the gluon polarisation in light mesons*, *Phys. Rev. D* **72** (2005) 094025 [hep-ph/0509213].
- [20] C.S. Fischer and R. Alkofer, *Nonperturbative propagators, running coupling and dynamical quark mass of Landau gauge QCD*, *Phys. Rev. D* **67** (2003) 094020 [hep-ph/0301094].
- [21] T.D. Cohen, *Functional integrals for QCD at nonzero chemical potential and zero density*, *Phys. Rev. Lett.* **91** (2003) 222001 [hep-ph/0307089].
- [22] P.J. Gunkel, C.S. Fischer and P. Isserstedt, *Quarks and light (pseudo-)scalar mesons at finite chemical potential*, *Eur. Phys. J. A* **55** (2019) 169 [1907.08110].
- [23] P.J. Gunkel, C.S. Fischer and P. Isserstedt, *Mesons at finite chemical potential and the Silver-Blaze property of QCD*, *J. Phys. Conf. Ser.* **1667** (2020) 012011 [1911.04399].
- [24] T.D. Cohen, *The Silver Blaze Problem in QCD*, 2601.21053.
- [25] A.L. Fetter and J.D. Walecka, *Quantum Theory of Many Particle Systems* (1971).
- [26] R. Alkofer, C.S. Fischer and F. Zierler, *Chiral symmetry restoration effects onto the meson spectrum from a Dyson-Schwinger/Bethe-Salpeter approach - DSE code and data release*, 2026. 10.5281/zenodo.18692770.